Source and development of large manganese enrichments above eastern Mediterranean sapropel S1

Anja Reitz,[1,2] John Thomson,[3] Gert J. de Lange,[1] and Christian Hensen[4]

Received 15 April 2005; revised 6 April 2006; accepted 14 April 2006; published 9 August 2006.

[1] The residual dark unit of the most recent eastern Mediterranean sapropel (S1) is usually overlain by sediments with enhanced concentrations of MnO_x in two separated layers. The variability and magnitude of the Mn enrichment at different locations and water depths indicate that Mn must have been added preferentially to sediments at intermediate (1–2 km) water depths. We propose a two-stage mechanism for the Mn enrichment that involves decreasing oxygenation with increasing water depth. This mechanism involves the loss of reduced Mn^{2+} from the deepest sediments (>2 km water depth) into overlying anoxic waters and a variable gain of MnO_x in sediments in contact with oxygenated waters at shallower depth. In the S1 unit that receives the extra MnO_x input, an upper higher Mn-enriched zone (>3 wt %) is maintained continuously at the top of the accumulating S1 unit because the pore waters are anoxic at shallow sediment depth while bottom waters are oxic to some degree. In a reactive-transport model, the Mn enrichment in the upper zone could not be supported by normal sediment diagenesis. Thus the MnO_x in the upper Mn horizon must have formed mainly in the water column. The MnO_x in the upper Mn-enriched zone adsorbed Mo and Li from seawater in a similar manner as other Mn-enriched oxic sediments, nodules, and crusts, with a Mn:Mo ratio of ~600:1, a Mn:Li ratio of ~750:1, and a $\delta^{98/95}Mo_{MOMO}$ of −2.5 ‰.

Citation: Reitz, A., J. Thomson, G. J. de Lange, and C. Hensen (2006), Source and development of large manganese enrichments above eastern Mediterranean sapropel S1, *Paleoceanography*, *21*, PA3007, doi:10.1029/2005PA001169.

1. Introduction

[2] Eastern Mediterranean sediments are generally C_{org}-poor, but discrete C_{org}- and sulfide-rich units known as sapropels formed repetitively in the sediment sequence over at least the past 3 Myr [*Rohling*, 1994]. A close relationship between sapropel formation and orbital precession-driven solar insolation variations has been interpreted to imply that an enhanced flux of monsoonal fresh water to the surface ocean must control sapropel formation in this semi-isolated basin [*Rossignol-Strick*, 1985; *Hilgen*, 1991; *Lourens et al.*, 1996; *Tuenter et al.*, 2003]. At present, C_{org}–poor sediments form [*Van Santvoort et al.*, 2002] because the basin's deep waters are ventilated regularly so that high O_2 contents are maintained throughout the water column [*Béthoux*, 1993; *Roether and Well*, 2001]. The scenario proposed for sapropel formation envisages that increased runoff leads to water column stabilization and probably to enhanced primary productivity [*Rohling*, 1994]. Deep-water dysoxia or anoxia then develops in the poorly ventilated deep waters to allow formation of sapropel with enhanced C_{org} preservation and diagenetic sulfide production in the sediments.

[3] Managense is a mobile element in sediments because of the ready interconversion of its different chemical species in response to early diagenetic redox changes that occur in sediment pore waters. The bacterial catalyzed remineralization of reactive organic matter in sediments reduces manganese oxide ($Mn(III,IV)O_x$) to soluble Mn(II) when sediment pore waters become suboxic or anoxic at depth. This Mn^{2+} diffuses in the pore waters until suboxic/oxic conditions preferentially in the presence of oxidizing bacteria are reencountered. At this boundary the main fraction of Mn^{2+} is again precipitated as MnO_x, either in the surficial sediments or in the overlying seawater. This behavior means that Mn is best suited to studies of changes in water column oxidation status during formation of the most recent sapropel (S1) between 9.5 and 6 ^{14}C kyr ago [*Mercone et al.*, 2000]. Two distinctly separated Mn-enriched zones are generally found in the sediments immediately above the visual expression of sapropel S1. The upper zone whose host sediment is about 5.7 kyr ^{14}C convention B.P. (interpolated [*Reitz et al.*, 2006]) has been related to changes in water column oxygenation that occurred at the end of this most recent sapropel episode. It has been important in quantifying the postdepositional oxidation that most S1 units have experienced since their formation [*De Lange et al.*, 1989; *Higgs et al.*, 1994; *Thomson et al.*, 1995, 1999; *Van Santvoort et al.*, 1996]. Pore water investigations have revealed that it is generally the lower of the two Mn-enriched zones that is forming actively, and that the maximum of this lower Mn-enriched zone marks the present limit of suboxic conditions in the sediments [*Van Santvoort et al.*, 1996].

[1]Department of Earth Sciences-Geochemistry, Faculty of Geosciences, Utrecht University, Utrecht, Netherlands.
[2]Now at Leibniz Institute of Marine Sciences at University of Kiel (IFM-GEOMAR), Kiel, Germany.
[3]Southampton Oceanography Centre, Southampton, UK.
[4]SFB574, Christian-Albrecht University Kiel, Kiel, Germany.

Copyright 2006 by the American Geophysical Union.
0883-8305/06/2005PA001169

[4] The genesis of the upper Mn-enriched zone (from here on upper Mn zone) that often contains higher Mn contents than the lower Mn-enriched zone (from here on lower Mn zone; but usually still <1 wt % Mn) is less certain [*Pruysers et al.*, 1993; *Thomson et al.*, 1995, 1999; *Van Santvoort et al.*, 1996]. Formation of the upper Mn zone usually appears to coincide with the end of sapropel formation, and it seems to be related in some manner to the resumption of ventilation and the return of high O_2 levels in bottom waters at the end of S1 sapropel times [*Thomson et al.*, 1995, 1999; *De Lange et al.*, 1999]. The upper Mn zone therefore formed before and is older than the corresponding lower Mn zone that is located a few cm deeper in the sediments. Cita and coworkers [*Cita et al.*, 1989; *Camerlenghi et al.*, 1992; *De Capitani and Cita*, 1996; *Hieke et al.*, 1996] also reported a prominent dark layer with variable Mn contents up to 22.8 wt % Mn above S1 in sediments of the diapiric crestal area on the Mediterranean Ridge. This layer has been termed the ''Marker Bed'', and its formation ascribed to an expulsion of hydrothermal fluid. There is a danger in considering any Mn feature as a marker bed, in the sense of a chronostratigraphic horizon that can be traced over a wide area, because of the early diagenetic mobility of Mn described above. *Thomson et al.* [1999] noted that the Marker Bed is similar to the upper Mn zone in published photographs, both in appearance and in position relative to the S1 sapropel, and they proposed that the Marker Bed and this Mn zone are equivalent. The unusually large Mn contents measured in some Marker Bed locality cores do however require further explanation.

[5] 1. Regarding the source and formation mechanism, large Mn enrichments might be diagenetic, i.e. formed within the sediments by early diagenesis. *Van Santvoort et al.* [1996] demonstrated that the lower Mn zone above the residual S1 unit is forming actively by this mechanism as outlined above. Very high Mn contents can be produced by this mechanism in surficial sediments if the surficial oxic zone is a few centimeters or less deep and Mn is continuously added to this thin oxic layer or zone [e.g., *Lynn and Bonatti*, 1965; *Shimmield and Price*, 1986; *Kadko et al.*, 1987]. In order to have produced the upper Mn zone in eastern Mediterranean sediments, this mechanism implies that finite bottom water O_2 contents were present during sapropel deposition. This would be required to maintain an oxic surficial layer in the sediments and prevent the escape of most of the Mn^{2+} from the sediments to bottom waters.

[6] 2. Large Mn enrichments might also be hydrogenetic, i.e., precipitated within the water column [e.g., *Force and Cannon*, 1988; *Frakes and Bolton*, 1992; *Calvert and Pedersen*, 1996]. If bottom water oxygen levels fall to sufficiently low but not necessarily zero levels, then significant amounts of Mn^{2+} from pore waters will diffuse out of the sediments and escape to bottom waters [*Balzer*, 1982; *Kristensen et al.*, 2003]. This process develops high Mn^{2+} concentrations in suboxic or anoxic water columns, as in the isolated basins of the Black Sea, the Cariaco Trench, silled fjordic basins [*Calvert and Pedersen*, 1996], and deep anoxic eastern Mediterranean brine basins [*De Lange et al.*, 1990]. A sharp solubility gradient of Mn exists along the oxic/anoxic interfaces in such water columns. Dissolved manganese contents in anoxic waters might be ~1000 times greater than in oxic surface waters where Mn concentrations are typically <10 ppb Mn because Mn^{2+} in solution is favored by the low Eh of anoxic waters [*Hem*, 1972; *Force and Cannon*, 1988]. If the stability of such an anoxic water column breaks down, then increased dissolved O_2 levels introduced with ventilation will precipitate dissolved Mn^{2+} as MnO_x that rains back down through the water column to the underlying sediments. Such a process occurs regularly in winter in the deep basins of the Baltic Sea [*Huckriede and Meischner*, 1996; *Sternbeck and Sohlenius*, 1997]. In order to produce the major upper Mn zone in eastern Mediterranean sediments a two-step process must be involved. First, low bottom water O_2 contents must have developed during sapropel deposition in order to allow Mn^{2+} to escape from sediments into the bottom waters, and second, an increase in ventilation at the end of sapropel formation must have introduced sufficient O_2 to reprecipitate this Mn^{2+}. If sapropel formation ended with a single ventilation event, then this latter mechanism might be expected to form the highest enrichment in the upper Mn zone at sites with the deepest water. This is not the case as will be seen below.

[7] 3. A further possibility is the hydrothermal formation of large Mn enrichments, i.e. produced through an emission of hydrothermal fluid. Manganese can be enriched in a range of forms in the vicinity of hydrothermal vents [*Roy*, 1992; *Mills and Elderfield*, 1995]. At active vents on the mid-ocean ridge system, Fe^{2+} tends to precipitate from black smoker plumes in close proximity to vents, whereas Mn^{2+} precipitates at a variety of near- and far-field sites. Manganese is sufficiently fractionated from Fe^{2+} that it can still be detected in plumes thousands of kilometers distant from the source vents [*Klinkhammer and Hudson*, 1986]. It therefore seems likely that the authigenic flux of Mn precipitated in the deep ocean contains a hydrothermal component [*Roy*, 1992]. To produce the upper Mn zone, this mechanism would imply a sufficiently high water column O_2 content to precipitate the emitted Mn, but any relationship in time to sapropel deposition would be fortuitous.

[8] Manganese enrichments formed by diagenetic, hydrogenetic, and hydrothermal mechanisms are expected to initially form some species of MnO_x. Once buried and as anoxic conditions develop over time, all types may contribute to surficial diagenetic MnO_x enrichments by the reduction mechanism outlined above.

[9] This work investigates two Mn zones observed above S1 sapropel units in a suite of 11 cores collected at different locations and water depths (650–3400 m) in the eastern Mediterranean basin (Figure 1). Particular emphasis is placed on cores with a major upper Mn zone in order to explore the source and mechanism of their formation.

2. Material and Methods

[10] Data obtained at the Utrecht and SOC laboratories at different times and by different analytical methods were assembled from cores selected to give a geographical and

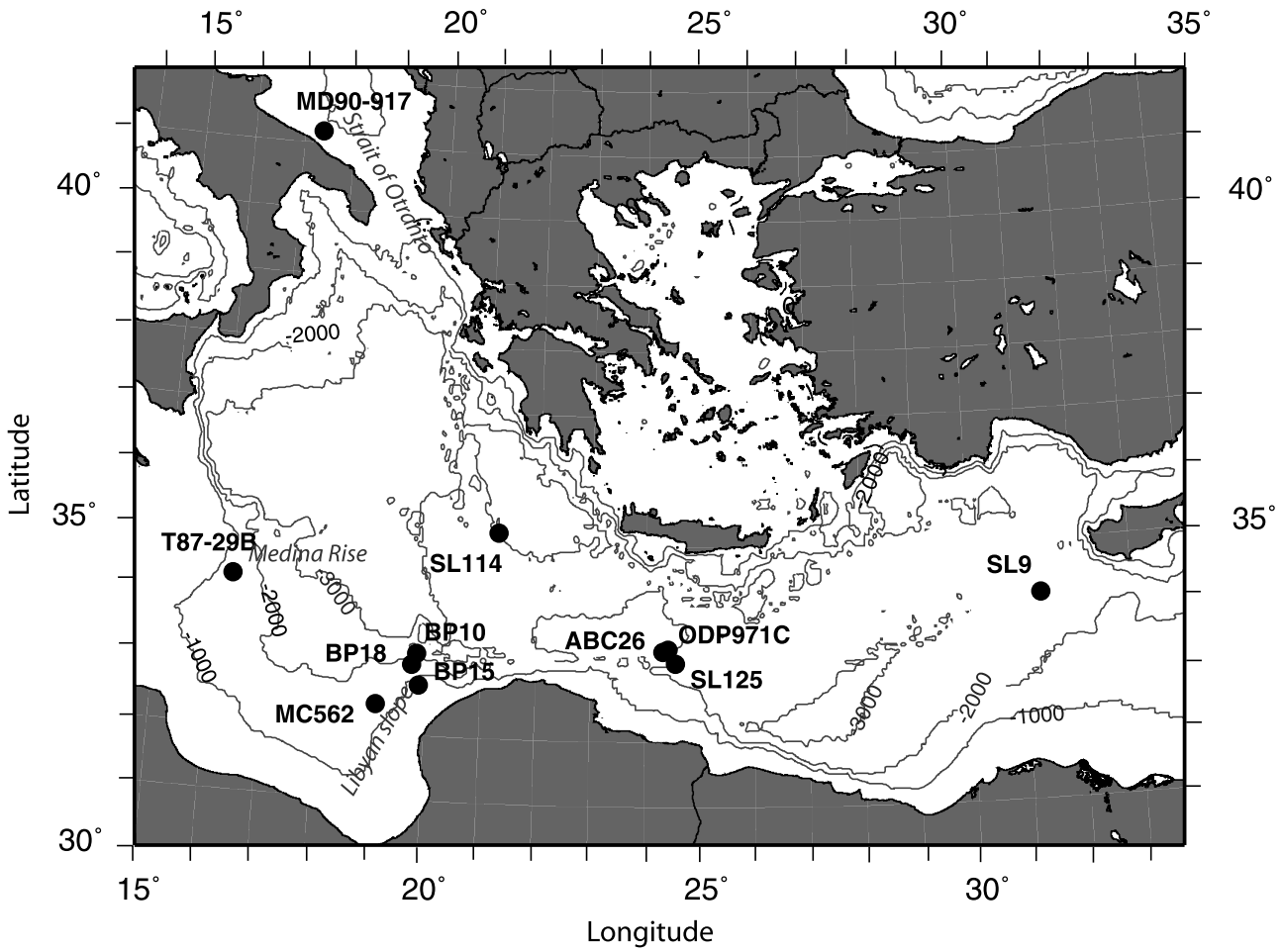

Figure 1. Map of the eastern Mediterranean Sea with locations of the cores investigated.

bathymetric coverage of the eastern Mediterranean basin (Figure 1 and Table 1). Those from box cores BP10, BP15, BP18, SL125, ABC26, SL9, and SL114 were analyzed by Inductively Coupled Plasma-Atomic Emission Spectrometry (ICP-AES) at 0.5 cm resolution after a three-step digestion to ensure total dissolution: (1) digestion of 125 mg of freeze-dried sediment in a mixture of 2.5 mL 3:2 concentrated $HClO_4$ and HNO_3 with 2.5 mL concentrated HF at 90°C; (2) evaporation of the solution to near dryness at 160°C; and (3) dissolution of the residual in 25 mL of 1 M HCl at 90°C. Ten samples from 9.5 to 14.5 cm in core BP18 were not completely digested in this manner; for these samples the procedure was applied to ~60 mg of sediment with an extra digestion step that involved evaporating the sample to near dryness with 5 mL concentrated HCl after step 2. Analyses of samples at 1 cm resolution from box core MC562 were performed by Inductively Coupled Plasma Mass Spectrometry (ICP-MS) after a three-step total digestion described by *Reitz et al.* [2004a]. Samples from box core T87-29B and hydraulic piston core

Table 1. Positions, Water Depths, and Other Details of the Cores Investigated

Core	Latitude, N	Longitude, E	Corer Type	Ship/Year	Water Depth, m	Maximum Mn Content in Upper Mn Zone, wt%
BP15	32°77.8′	19°87.6′	box	R/V *Pelagia*/2001 (Biopass)	665	0.13
MD90-917	41°18′	17°37′	piston	R/V *Marion Dufresne*/1990	1010	3.3
MC562	32°46.3′	19°11.5′	multi	R/V *Meteor*/2001 (M51-3)	1391	9.4
T87-29B	34°32.7′	16°34.0′	box	R/V *Tyro*/1987	1530	4.7
BP18	33°10.0′	19°73.3′	box	R/V *Pelagia*/2001 (Biopass)	1850	24.6
SL125	33°39.4′	24°33.0′	box	R/V *Professor Logachev*/1999 (Smilable)	1946	2.9
BP10	33°22.2′	19°76.7′	box	R/V *Pelagia*/2001 (Biopass)	2108	0.88
ABC26	33°21.3′	24°55.7′	box	R/V *Tyro*/1987	2150	1.2
ODP971C	33°42.8′	24°42.1′	piston	R/V *JOIDES Resolution*/1996 (ODP Leg 160)	2152	13.6
SL9	34°17.2′	31°31.4′	box	R/V *Professor Logachev*/1999 (Smilable)	2302	2.4
SL114	35°17.2′	21°24.5′	box	R/V *Professor Logachev*/1999 (Smilable)	3390	0.74

Table 2. Sequential Extraction Procedure

Step	Repeats	Extractant	Shaking Time, hours	Phase Extracted	Reference
1	x1	25 mL demineralized water	2	dried pore water salts	
2	x2	25 mL 1 M $MgCl_2$; pH8 25 mL demineralized water rinse	4	absorbed ions	*Ruttenberg* [1992]
3	x5	25 mL 2 M NH_4Cl; pH7	minimum 4	carbonates	*De Lange* [1992]
4	x2	25 mL 0.17 M Na-citrate/0.6 M $NaHCO_3$/0.11 M ascorbic acid; pH 8	16	poorly crystalline/amorphous (hydr)oxides	*Kostka and Luther* [1994]
5	x1	25 mL 1 M Na-acetate; pH 5 (buffered with acetic acid)	16	residual carbonates	*Rutten et al.* [1999]
6	x2	25 mL 0.2 M Na-citrate/0.35 M Na-acetate (pH 4.8) plus 1.25 g Na-dithionite	5	crystalline (hydr)oxides	*Kostka and Luther* [1994]
	x2	25 mL demineralized water rinse			
7		total digestion		residual minerals and pyrite	*Lord* [1982]

971C from Ocean Drilling Program (ODP) Leg 160 were analyzed by ICP-AES after a 1:5 fusion with $LiBO_2$ [*Totland et al.*, 1992] at 0.5 and 1 cm resolution, respectively. Further analyses of Mo and Li in selected samples from these two cores were performed in the manner described above for core BP18. For the different procedures, sample duplicates, international standards, and in-house standards were processed to monitor the precision (by duplicates) and accuracy (by standards) of the analyses.

[11] Organic carbon content was determined according to the method described by *van Santvoort et al.* [1996]. International and in-house standards and duplicates were processed to monitor precision and accuracy.

[12] A sequential extraction with different solutions (Table 2) was applied to five 125 mg samples of box core BP18; one background sample from the sediment above the upper Mn peak (5.5–6 cm), three from the upper Mn peak (10.5–11, 12–12.5, and 13–13.5 cm), and one from the lower Mn peak (17–17.5 cm). All samples and two standards (international standard MAG-1 and an in-house manganese nodule standard) were processed in duplicate to monitor the precision of the sequential extraction. Recovery with respect to the standard total element concentrations of Mn, Ba, Fe, and Li was 99%, 94%, 99%, and 107%, respectively.

[13] Pore water analyses of BP10 were done by ICP-MS after onboard sampling of the box core at in situ temperature (~13°C) in a nitrogen-filled glove box and centrifugation to separate pore waters. Sample duplicates were analyzed to monitor over all precision and analyses were done in triplicate; reproducibility was better than 10% for Mn concentrations <1.5 μmol L^{-1} and better than 5% for concentrations >1.5 μmol L^{-1}.

[14] Determination of molybdenum isotope fractionation was performed at the University of Bern by double-spike inductively coupled plasma-multicollector mass spectrometry by methods described by *Siebert et al.* [2001].

[15] Bulk element data (e.g., Fe, Mn, and Ba) are normalized to Al to take account of fluctuations in aluminosilicate content, on the assumptions that the element/Al ratios in detrital material are relatively constant, and that increases in these ratios above detrital levels indicate diagenetic enhancements of the redox-sensitive elements [e.g., *Van Os et al.*, 1994; *Van der Weijden*, 2002]. For higher concentrations of Mn in the large upper Mn zone, a major fraction of the Ba appears to be associated with MnO_x rather than present as biogenic barite. As barite is an important indicator for sapropel formation, a correction for this MnO_x-associated Ba is needed. The Ba associated with the maximum upper MnO_x ($(Ba/Mn)_{mum}$ ~0.0031) was determined by sequential extraction; this ratio has been used to correct the Ba/Al ratio in cores with a high Mn concentration in the upper Mn zone (>3 wt % Mn; section 3.2), using

$$Ba/Al = \left(Ba_{tot} - Mn_{tot}(Ba/Mn)_{mum}\right)/Al_{tot} \quad (1)$$

where Ba_{tot}, Mn_{tot}, and Al_{tot} are the element concentrations in bulk sediments determined from total digestion. Although Ba_{excess} values could have been calculated [*Reitz et al.*, 2004b], we preferred to use Ba/Al for the correction because the cores are from a wide variety of locations showing detrital background Ba/Al values between 0.0021 (SL9) and 0.0059 (MC562 on the Libyan shelf).

2.1. Model Description

[16] A Mathematica®-based, one-dimensional, reactive transport model scheme was composed to quantify MnO_x formation in the sediments. A similar model setup was described by *Hensen and Wallmann* [2005]. The model enables for the calculation of sedimentation, molecular diffusion, and degradation of organic matter. Rates of C_{org} degradation (R_{Corg} in wt % yr^{-1}) are given by

$$R_{C_{org}}(x) = k_{C_{org}}\left[C_{org}\right], \quad (2)$$

where k_{Corg} is the kinetic constant for the degradation of reactive C_{org} yr^{-1} and [Corg] is the concentration of reactive organic carbon in wt % that reaches the sediment surface.

[17] Likewise, the rate of Mn^{2+} oxidation (R_{MnOx} in wt % yr^{-1}) by oxygen is calculated as

$$R_{MnOx}(x) = k_{MnOx}[O_2]\left[Mn^{2+}\right], \quad (3)$$

where k_{MnOx} is the kinetic constant for Mn^{2+} oxidation in cm^3 μmol^{-1} yr^{-1}, and $[O_2]$ and $[Mn^{2+}]$ are the corresponding concentrations in μmol cm^{-3} of pore solution.

[18] To keep the model simple, the relevant processes of organic carbon degradation were reduced to oxic respiration

Table 3. Summary of The Parameter Values Used in the Model

Parameter	Symbol	Value	Reference
Sedimentation rate (S1 times)	SR	5.0 cm kyr^{-1}	this study
Sedimentation rate (post-S1 times)	SR	2.0 cm kyr^{-1}	this study
Porosity (constant)	ϕ	0.65	this study
Grain density	d_s	2.65 g cm^{-3}	this study
Degradation constant of C_{org}	K_{Corg}	0.005 yr^{-1}	this study
Monod constant for oxic respiration	k_{O2}	0.008 mmol dm^{-3}	this study
Monod constant for manganese oxide reduction	k_{Mn}	10.0 mmol dm^{-3}	this study
Inhibition constant for manganese oxide reduction	k_{IO2}	0.001 mmol dm^{-3}	this study
Kinetic constant for Mn^{2+} oxidation	k_{MnOx}	1×10^6 dm^3 $mmol^{-1}$ yr^{-1}	*Boudreau* [1996]
Temperature	T	13.0°C	*Van Santvoort et al.* [1996]
Boundary conditions			
Organic carbon at the sediment surface (S1 times)	$[C_{org}]$	2.5 wt%	this study
Organic carbon at the sediment surface (post-S1 times)	$[C_{org}]$	0.3 wt%	this study
Dissolved O_2 at the sediment surface (S1 times)	$[O_2]$	0.0001 mmol dm^{-3}	this study
Dissolved O_2 at the sediment surface (post-S1 times)	$[O_2]$	0.2 mmol dm^{-3}	*Van Santvoort et al.* [1996]
Dissolved Mn^{2+} at the sediment surface (S1 times)	$[Mn^{2+}]$	0.25 mmol dm^{-3}	according to *Kulik et al.* [2000]
Dissolved Mn^{2+} at the sediment surface (post-S1 times)	$[Mn^{2+}]$	0.0 mmol dm^{-3}	this study
Dissolved Mn^{2+} below the Mn peaks (present-day)	$[Mn^{2+}{}_{PD}]$	0.004 mmol dm^{-3}	this study
MnO_x input at the sediment surface	$[MnO_x]$	0.06 wt %	this study

and manganese-oxide reduction. These processes were implemented by rate laws using Monod-type kinetics:

$$R_{O_2}(x) = \frac{138}{106} R_{C_{org}} \frac{[O_2]}{(k_{O_2} + [O_2])} - R_{MnOx}, \quad (4)$$

$$R_{Mn}(x) = 2R_{C_{org}} \frac{[MnO_x]}{(k_{Mn} + [MnO_x])} \frac{k_{IO2}}{(k_{IO2} + [O_2])} - R_{MnOx}, \quad (5)$$

and

$$R_{MnOx}(x) = -2k_{C_{org}}[C_{org}] \frac{87}{12} \frac{[MnO_x]}{(k_{Mn} + [MnO_x])} \frac{k_{IO2}}{(k_{IO2} + [O_2])} + R_{MnOx}, \quad (6)$$

where R_{O2}, R_{Mn}, and R_{MnOx} are the rate of oxidation, manganese reduction, and manganese oxidation in mmol dm^{-3} yr^{-1} and wt % yr^{-1} (for R_{MnOx}), $[MnO_x]$ is the species concentration in mmol dm^{-3}, k_{O2} is the Monod constant for oxic respiration in mmol dm^{-3}, k_{Mn} is the Monod constant for manganese-oxide reduction in mmol dm^{-3}, and k_{IO2} is the inhibition constant for manganese-oxide reduction in mmol dm^{-3}. A summary of all parameter values used is given in Table 3.

3. Results and Discussion

3.1. General Characteristics of Mn-Enriched Horizons Above Sapropel S1

[19] Interpretations of C_{org}, Ba/Al, Fe/Al, and Mn/Al profiles through S1 units were reviewed by *Thomson et al.* [1999], and the data for the new cores discussed in this section have many similarities to the limited number (about a dozen) of eastern Mediterranean cores containing S1 for which detailed inorganic data have been reported. A set of five parameters is presented for core BP10 (Figure 2) to illustrate the geochemical criteria that define the original and residual S1 boundaries. Mn/Al and Fe/Al profiles are also shown for cores BP15, ABC26, SL9, and SL114, where the thickness of the visual S1 unit and the amount of oxidation that occurred since deposition were evaluated in a similar manner to that applied to core BP10 (Figure 2).

[20] Unless S1 units are from areas of unusually high sediment accumulation rates [*Mercone et al.*, 2000, 2001], they are generally thinner than the unit originally laid down, because of postdepositional oxidation. This oxidation greatly diminished or destroyed the original C_{org} and sulfide contents in the upper part of the sapropel and thus lightened the characteristic dark color that accompanies high C_{org} and S contents in sapropels [*De Lange et al.*, 1989, 1994; *Higgs et al.*, 1994; *Thomson et al.*, 1995, 1999; *Van Santvoort et al.*, 1996]. Fortunately, biogenic Ba (as barite) that accompanied settling C_{org} appears to be preserved in the sapropels, even after the C_{org} has been extensively oxidized [*Thomson et al.*, 1995]. Thus the positions and shapes of the Ba/Al and Mn/Al profiles allow deduction of the original thickness of S1 [*Thomson et al.*, 1995, 1999; *Van Santvoort et al.*, 1996; *Mercone et al.*, 2000; *Rutten and De Lange*, 2002] (Figure 2). For all cores shown in Figure 2, except core BP15 from the shallowest water depth, the upper Mn/Al peak occurs exactly at the top of the zone of high Ba/Al values that marks the original S1 unit, as seen in the detailed profiles of core BP10; the lower Mn/Al peak is situated immediately above the zone of high C_{org}. This is evidence of the postdepositional oxidation of sapropel S1 that occurred between the two Mn peaks over the last 6 kyr. The pore water Mn^{2+} profile (Figure 2) indicates continuing suboxic/anoxic reduction of MnO_x in underlying sediments that fuels formation of the lower Mn zone.

[21] There is little or no evidence of Fe enrichment associated with the upper Mn peak in these cores. By contrast, a clear enrichment of Fe is associated with the lower (diagenetic) Mn peak in all cores. This indicates that the precipitation of Mn oxide and Fe oxyhydroxide is fueled

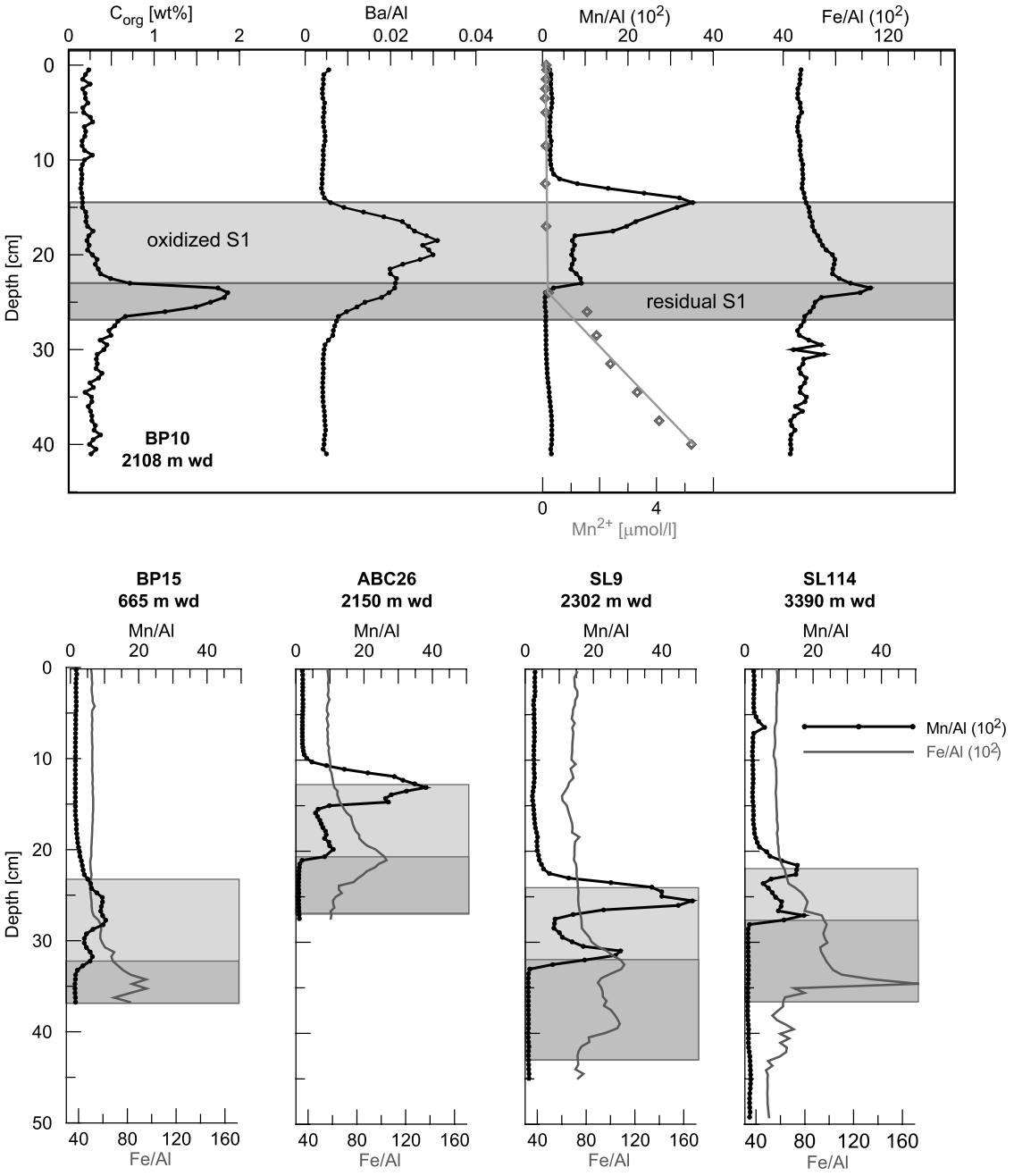

Figure 2. (top) Element concentrations (C_{org}) and ratios (Ba/Al, Mn/Al and Fe/Al) in the sediment and pore water Mn^{2+} concentration versus depth in core BP10. These profiles illustrate how geochemical data are used to define the original S1 thickness and divide it into oxidized and residual sections according to criteria described in the text (section 3.1). The residual S1 and the oxidized S1 zones are illustrated by the dark and light grey shadings, respectively. Original element concentrations are $\mu g\ g^{-1}$ unless otherwise indicated; 10^2 indicates that the ratio was multiplied by 100. (bottom) Mn/Al and the Fe/Al ratio profiles versus depth for four cores from different eastern Mediterranean locations and water depths. Shadings as above indicate residual and oxidized S1 zones in each core.

by Mn^{2+} and Fe^{2+} diffusing up from below and by bottom water O_2 penetrating into the sediment [*De Lange et al.*, 1989; *Van Santvoort et al.*, 1996; *Passier et al.*, 2001; *Rutten and De Lange*, 2003]. The lower Mn zone with associated Fe formed after S1 formation due to the penetration of the oxidation front into the sediment. This process continues at present, except at very shallow water sites (~<500 m). The behavior of Fe in sapropels differs from Mn in that Fe and S form pyrite. High Fe/Al values in the visually observable sapropel, where Mn values are low and C_{org} and S values are high, indicate the presence of pyrite [*Passier et al.*, 1996]. Passier et al. also reported sulfide

formation in excess of the available Fe for sapropel S1. This excess may not only have resulted in the downward sulfidization process and associated consumption of all available Fe^{2+} during S1 formation, but may also have resulted in a HS^- flux into the water column. The latter would have maintained low Fe^{2+} concentrations in the water column.

3.2. An Upper Mn layer in Oxic Conditions Above Sapropel S1

[22] Section 3.1 demonstrated that S1 units in different cores display some compositional variability and consistent evidence for postdepositional oxidation after their formation. Among the major elements, Mn shows the greatest concentration variations in S1 units. In this section, five cores are examined that have a much larger upper Mn peak than the <1 wt% levels (Figure 2). Core BP18 from the Libyan slope has the highest Mn concentration (24.6 wt %) in the upper Mn peak yet reported for the eastern Mediterranean.

3.2.1. Libyan Continental Slope

[23] Core MC562 was recovered west of Cape Sirte in 1391 m water depth and has a maximum Mn content of 9.4 wt % in the upper Mn zone. Core BP18 was recovered northwest of Cape Sirte at 1850 m and has a maximum Mn content of 24.6 wt % in the upper Mn zone. XRD analysis of the core BP18 sample with the highest Mn concentration established birnessite as the main Mn phase, and an absence of Mn-carbonate minerals (rhodochrosite/kutnahorite) (C. Vogt, personal communication, 2004). This finding is supported by sequential extractions that reveal that nearly all the Mn in the upper zone is extracted in the poorly crystalline and amorphous oxide/oxyhydroxide fraction (Figure 3).

[24] The uncorrected Ba/Al profile of core BP18 displays a narrow peak that coincides exactly with the upper Mn peak (Figure 3). For the samples discussed in this section that have Mn concentrations >0.5 wt%, a correction for Ba absorbed to MnO_x was made because sequential extraction confirmed that some Ba is associated with the poorly crystalline/amorphous oxide fraction and is therefore unrelated to biogenic barite (see section 2). The Fe/Al profiles of both cores display small Fe enrichments that correspond to the upper Mn enrichment. This is interpreted as a sorption of Fe^{2+} on MnO_x [*Koschinsky and Halbach*, 1995] because sequential extraction of core BP18 samples released a fraction of the total Fe from the sediments of the upper Mn zone in the absorbed ion fraction, a feature that is not observed in samples from above or below the upper Mn zone. It seems that sorption of Fe^{2+} onto MnO_x can be discerned when Mn concentrations exceed 5 wt % (compare Figures 3 and 5; MC562 with ~9 wt % Mn and T87-29B with ~5 wt % Mn). Both Fe/Al profiles show a clear and distinct enrichment of Fe that corresponds with the lower Mn enrichment. However, the fraction of Fe released in the poorly crystalline/amorphous (oxyhydr)oxide fraction by sequential extraction of the BP18 samples increases in the lower Mn zone, whereas there is negligible Fe leached with the absorbed ion fraction (17.5 cm, Figure 3).

[25] *Casford et al.* [2003] reported the presence of benthic foraminifera throughout S1 for core MC562. They postulated conditions of either continuous dysoxia or intermittent ventilation at ~2000 m water depth. Conversely, benthic foraminifera are absent between ~28 cm (~8.73 kyr; interpolated) and 14 cm (5.5 kyr, direct radiocarbon dating) sediment depth in core BP18, implying extensive anoxia during sapropel formation.

3.2.2. Marker Bed Area

[26] Box core SL125 with a maximum Mn content of 2.9 wt % in the upper Mn zone was retrieved from 1946 m water depth in the diapiric summit area of the Mediterranean Ridge south/southwest of Crete where high Mn values have been reported [*Cita et al.*, 1989; *De Capitani and Cita*, 1996]. The profiles in this core are very similar to those discussed above (Figures 2 and 3), with the exception that the upper Mn peak is much broader (Figure 4) than the others discussed in this paper. As in the other examples, this peak corresponds exactly to the top of the S1 unit.

[27] ODP hydraulic piston core 971C is located in the circular depression or "moat" that surrounds the Napoli mud dome in the Marker Bed area. The S1 unit in this core is unusual in that it is ~65 cm thick, whereas all other S1 units investigated are 15–20 cm thick (Figures 2, 3, and 5). The ODP shipboard description of 971C notes that the S1 unit is "expanded", but our interpretation, based on micropaleontology (E. J. Rohling, personal communication, 2004) and inorganic chemistry is that the unusual thickness of this S1 unit is due to a redeposition near the end of sapropel time of ~50 cm of S1 sapropel sediment, as indicated in Figure 4.

[28] The point of interest of core 971C S1 for this study is that the upper Mn peak is large and very sharp, with the upper and lower Mn peak maxima containing 14.2 and 0.62 wt % Mn (Figure 4). The upper peak corresponds to the top of the high Ba/Al values, and the separation of the maxima at 31.5 and 36.5 cm indicates 5 cm of postdepositional oxidation, which is similar to the oxidation depth seen in most other S1 units (e.g., BP10 in Figure 2). Although different hydrogenetic, diagenetic, or diapiric (deep-seated) possibilities for Mn supply can be invoked for a highly enriched upper Mn zone at this locality, this Mn zone must have formed very late in S1 times, if it was caused by redeposition (Figure 4). It is most likely that the upper Mn zone represents a thin surficial diagenetic MnO_x layer that formed from a pore water flux of Mn^{2+} that was generated from the redeposited sapropel sediment in this unusually thick S1 unit. This interpretation requires that bottom waters were oxic. The unusual thickness of the S1 unit in comparison with the other cores from the Marker Bed area (ABC26 and SL125, Figures 2 and 4) suggests that a redeposition event is the major factor that produced such a highly enriched upper Mn zone. Its sharpness demonstrates the rapidity of MnO_x remobilization and redistribution.

3.2.3. Medina Rise Area

[29] Core T87-29B was retrieved from a water depth of 1530 m depth on Medina Rise and has a maximum Mn content of 4.7 wt % in the upper Mn zone [*Rasmussen*, 1991; *Troelstra et al.*, 1991]. The separation of the upper and lower Mn zones related to postdepositional oxidation is similar to that seen in the other cores, but an important difference is that the upper Mn zone is located in a slightly different position. Its maximum is located 2 cm below the top of the zone of high Ba/Al values that define the full S1 sapropel,

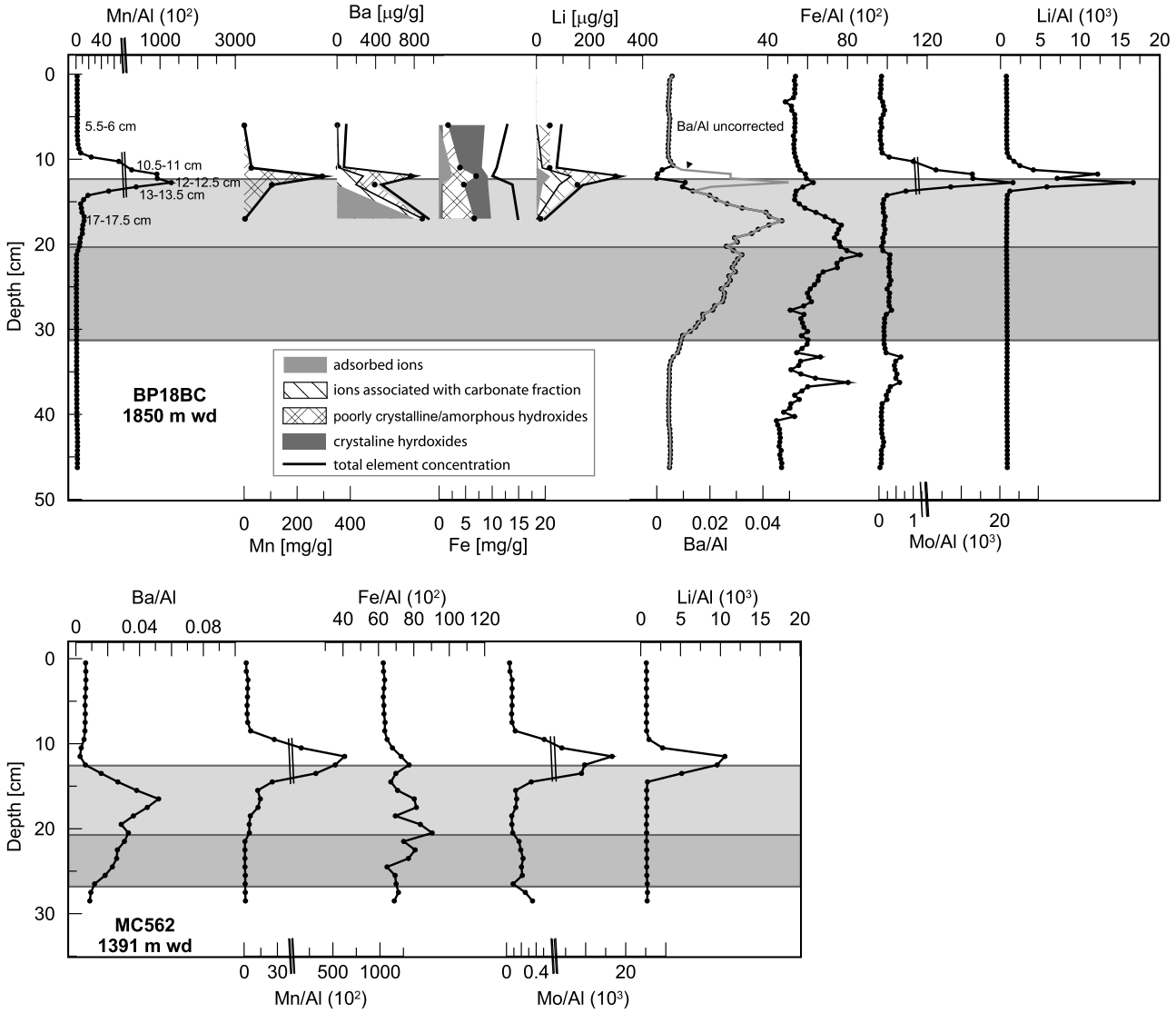

Figure 3. (top) Element ratios versus depth in core BP18 and elemental concentrations of Mn, Ba, Fe, Li (cumulative presentation) in five samples analyzed by sequential extraction. The amount of Ba sorbed on MnO_x is shown as a grey line on the Ba/Al plot. (bottom) Element ratio profile versus depth for core MC562. Shadings as in Figure 2 indicate the residual and oxidized S1 zones. Note that Mn/Al and Mo/Al plots have an *x* axis change of scale. All element concentrations are in μg g^{-1}; 10^2 and 10^3 indicate that the ratio was multiplied by 100 and 1000, respectively.

rather than exactly on its upper boundary (Figure 5). According to a hydrogenetic origin for Mn in the upper Mn zone, this zone would have formed at the seafloor before the end of sapropel time. Alternatively, if the upper layer formed diagenetically, it would represent oxygen penetration into the surface-sediment layer at this shallower water location during the last phase of sapropel formation.

3.3. Molybdenum Sorption on Manganese Oxide (MnO_x)

[30] The large Mn peaks discussed above are accompanied not only by enrichments of adsorbed Ba and Fe (section 3.2), but also by variable enrichments of several other elements. The elements that exhibit the most pronounced and consistent enrichments are Mo and Li. All the cores with a large Mn peak in the upper Mn zone display an exact coincidence of Mn/Al, Mo/Al, and Li/Al maxima, with the Mo and Li enrichments clearly dependent on the magnitude of the Mn peak (Figures 3, 4, and 5).

[31] Molybdenum can be concentrated from seawater by reduction in strongly reducing or sulfidic sediments, because it is readily incorporated into authigenic sulfides [*Huerta-Diaz and Morse*, 1992; *Crusius et al.*, 1996; *Helz et al.*, 1996; *Vorlicek and Helz*, 2002; *Sundby et al.*, 2004]. High Mo contents are therefore always observed in unoxidized sapropel units along with high S and Fe contents and low Mn contents (e.g., Figure 3, 4, and 5).

[32] In contrast, an estimated 47–85% of the total Mo removal from the ocean occurs under oxic conditions by pelagic sediments [*Bertine and Turekian*, 1973; *Morford and*

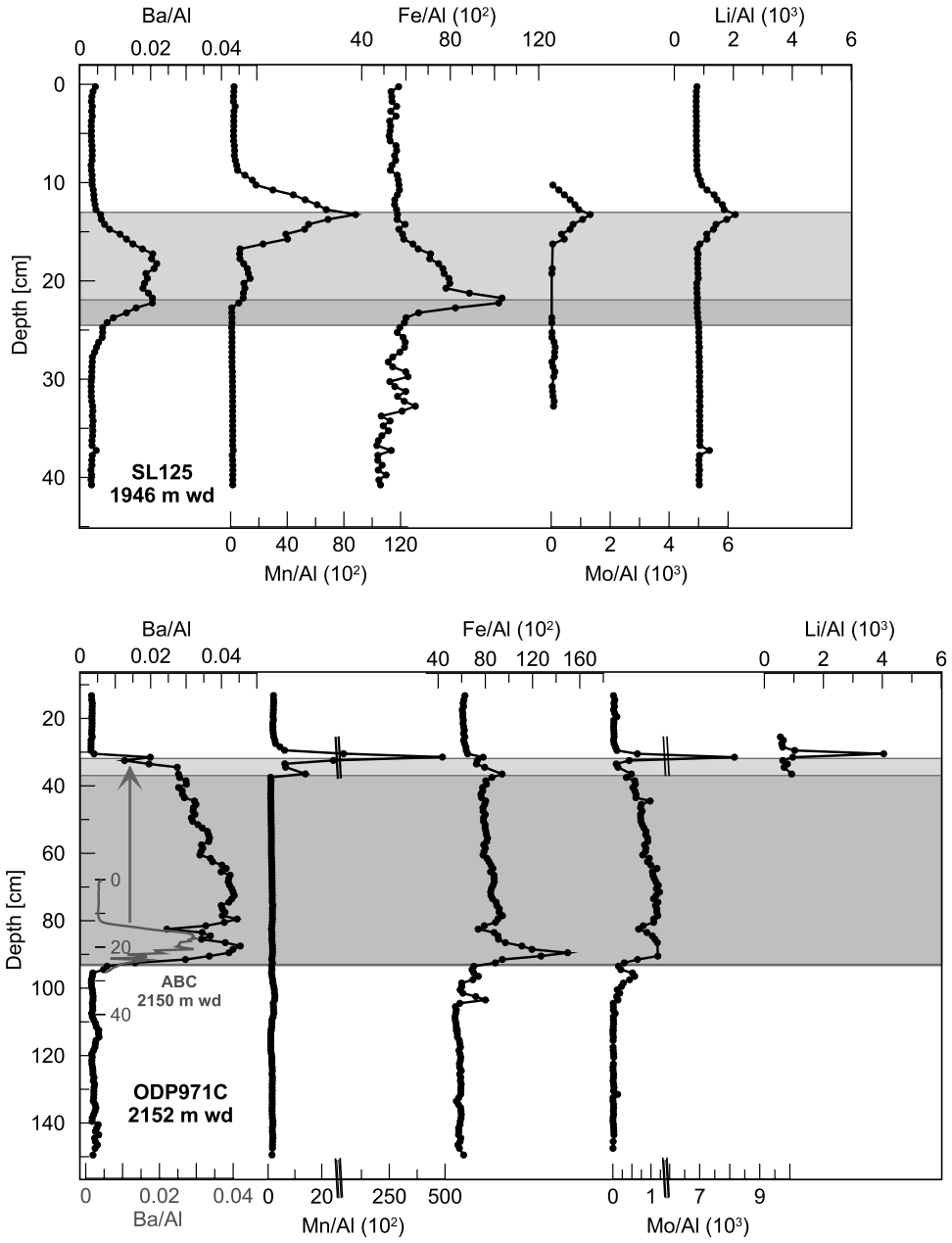

Figure 4. (top) Element ratios versus depth in core SL125. (bottom) Element ratios versus depth in core ODP971C. The Ba/Al profile of nearby core ABC26 is overlain in grey to indicate the inferred position of the original S1 sapropel in this core that is overlain with ~50 cm of redeposited sapropel (arrow) on top. Note that the Mn/Al and Mo/Al plots exhibit an *x* axis change of scale. Original element concentrations are in μg g^{-1}; 10^2 and 10^3 indicate that the ratio was multiplied by 100 and 1000, respectively. Shadings as in Figure 2 indicate the residual and oxidized S1 zones.

Emerson, 1999]. *Shimmield and Price* [1986] summarized evidence for the scavenging and uptake of Mo by oxic Mn-containing sediments, Mn-containing particulate material, and ferromanganese nodules. It was demonstrated that the Mn:Mo mass ratio in Mn-enriched oxic sediments, nodules, and crusts is consistently ~500:1 up to 25 wt % Mn (500 μg g^{-1} Mo [*Takematsu et al.*, 1985; *Shimmield and Price*, 1986; *Calvert and Pedersen*, 1993]). Unlike Mo enrichments with sulfide, burial and preservation of these Mo enrichments in the sedimentary record is not expected because of reductive dissolution of MnO_x during burial. *Shimmield and Price* [1986] suggest that Mo adsorbed by MnO_x is preferentially released and lost to solution when the Mn[IV] and Mn[III] in MnO_x are reduced to Mn[II]. This contrasts with the behavior of Mn itself, because residual MnO_x can adsorb Mn^{2+} after reductive release to solution.

[33] Most of the Mn in both zones above the residual S1 is present as MnO_x (section 3.2.1) and is therefore also

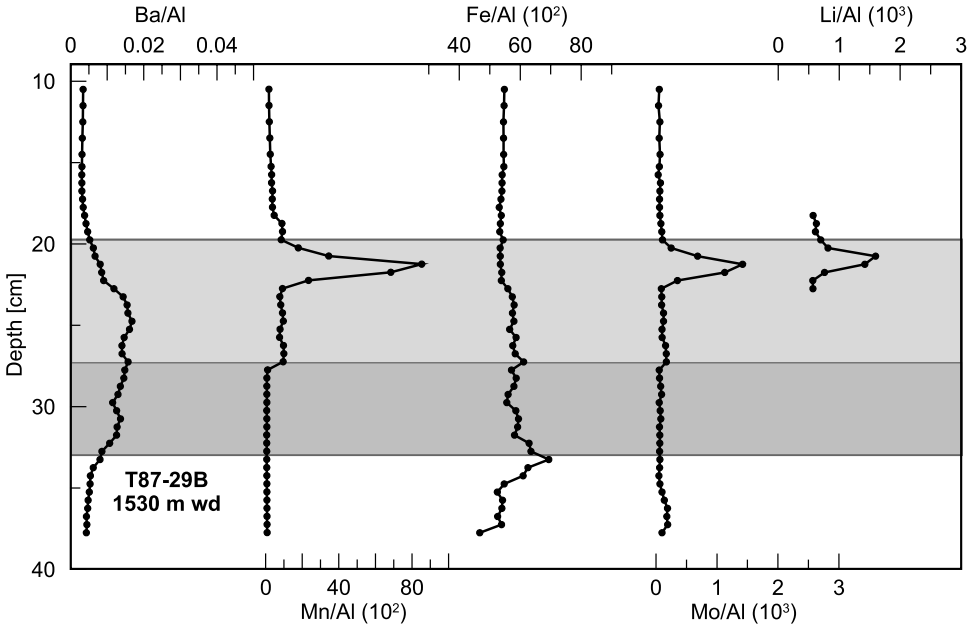

Figure 5. Element ratios versus depth in core T87-29B. Original element concentrations are in $\mu g\ g^{-1}$; 10^2 and 10^3 indicate that the ratio was multiplied by 100 and 1000, respectively. Shadings as in Figure 2 indicate the residual and oxidized S1 zones.

expected to adsorb Mo. In the oxic sediments above the residual sapropel, where Mn contents exceed 1500 $\mu g\ g^{-1}$ (0.15 wt %), Mo correlates linearly with Mn (average r^2 and n of the 5 cores discussed in this section is 0.97 and 8, respectively). The average enrichments of ~600 (MC562 419:1; BP18 696:1; SL125 769:1; ODP971C 617:1; T87-29B 620:1) is slightly higher than the 500:1 ratio reported by *Shimmield and Price* [1986]. The average Mn:Mo ratio of 600:1 appears to be the ratio for Mo adsorbed from eastern Mediterranean bottom waters on to MnO_x.

[34] Molybdenum isotope fractionation was determined for two samples from the upper Mn zone of BP18. The sample with the highest Mn concentration at 12–12.5 cm has a Mo isotope composition of $\delta^{98/95}Mo_{MOMO} = -2.6$ ‰ (±0.1) and the sample immediately below has a value of −2.4 ‰ (±0.1). These isotopic compositions are distinctly offset from the values found by *Siebert et al.* [2003] for ocean waters ($\delta^{98/95}Mo_{MOMO} = 0$ ‰) and reducing sediments ($\delta^{98/95}Mo_{MOMO} = -1.8$ to −0.5 ‰), but lie between the estimated mean crustal composition ($\delta^{98/95}Mo_{MOMO} = -2.3$ to −2 ‰) and Fe-Mn crusts and pelagic sediments ($\delta^{98/95}Mo_{MOMO} = -2.7$ to −2.9 ‰). The preferential sorption of lighter Mo isotopes to the upper Mn peak MnO_x therefore appears consistent with sorption from seawater under oxic conditions (T. Nägler, personal communication, 2004), although more measurements are required for a fuller interpretation.

3.4. Lithium Sorption on Manganese Oxide (MnO_x)

[35] Alkali elements like lithium are unaffected by redox reactions [*James and Palmer*, 2000] and most of the uptake of Li into particulate material occurs in the water column before burial in sediments [*Zhang et al.*, 1998]. In order to establish the authigenic fraction in the large upper Mn zone, Li_{excess} was calculated as

$$Li_{excess} = Li_{tot} - \left(Al_{tot}(Li/Al)_{det}\right), \quad (7)$$

because of a relatively large Li-clay contribution with a constant Li/Al ratio. Li_{tot} is the bulk Li concentration and $(Li/Al)_{det}$ is the Li concentration associated with the clay minerals, determined by sequential extraction as 0.0007. The average Mn:Li_{excess} ratio is ~750:1 (MC562 652:1; BP18 898:1; SL125 724:1; T87-29B 797:1) within the upper Mn peak. A positive correlation (except core T87-29B) of Li_{excess} and Mn contents (the average r^2 and n of the first three cores is 0.92 and 9 and that of the last core is 0.24 and 3, respectively) for samples formed under oxic conditions has not been previously reported to our knowledge. Some but by no means all hydrothermal samples rich in Mn oxides also show distinct enrichments of Li [*Hodkinson et al.*, 1994; *Glasby et al.*, 1997; *Koschinsky and Hein*, 2003; *Dekov et al.*, 2003]. In fresh precipitates from seawater, *Sato et al.* [1989] found that concentrations of alkali and alkaline earth elements were higher in Mn oxides than in Fe(III) oxides. The ionic radii of Li^+ and Mo^{6+} are the same (0.68 Å), and are believed to substitute for Mn^{4+} with an ionic radii of 0.62 Å [*Koschinsky and Hein*, 2003]. On the basis of the sequential extractions, the largest Li fraction was released in step 4 that dissolves poorly crystalline/amorphous oxides (Figure 3), but a significant fraction is also released in step 3 that dissolves carbonates. According to *Koschinsky and Hein* [2003], who found similar Li behavior in a leaching investigation, Li may be present either as a loosely bound fraction or as a discrete Li phase. In core BP18, the main Li_{excess} fraction is associated with the poorly crystalline/amorphous-oxide

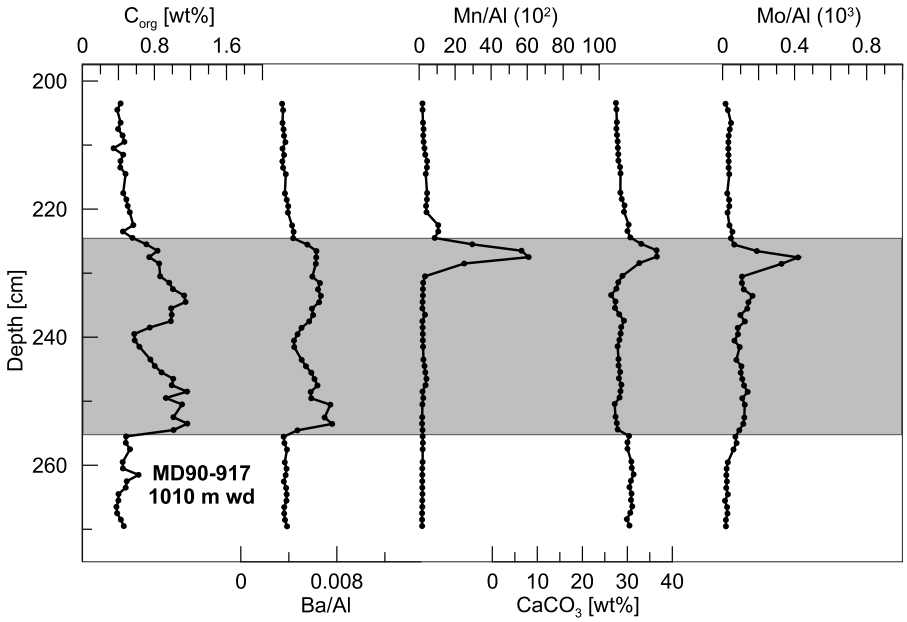

Figure 6. C_{org} and $CaCO_3$ contents (wt %) and element ratios versus depth in core MD90-917. Original element concentrations are in $\mu g\ g^{-1}$; 10^2 and 10^3 indicate that the ratio was multiplied by 100 and 1000, respectively. The residual S1 is indicated by the grey shading (this S1 example is so rapidly accumulated that it has no oxidized section).

phase and a minor fraction is found as the easily exchangeable phase/absorbed ions. Earlier investigations [*Gieskes*, 1983; *Zhang et al.*, 1998; *James and Palmer*, 2000] showed that Li is a readily exchangeable ion because seawater Li deposited along with marine sediments is readily displaced from the solid to solution by less hydrated cations like NH_4^+. Thus Li may be adsorbed directly from seawater or from Li released from underlying sediments.

3.5. An Upper Mn Layer Now Located in Anoxic Conditions: S1 Sapropel in Core MD90-917

[36] *Mercone et al.* [2000, 2001] reported that a single layer of high Mn content (3.3 wt %) exists in the S1 sapropel of core MD90-917 recovered from a depth of 1010 m in the Otranto Strait, Adriatic Sea (Figure 6). At this locality the sediments accumulate so rapidly that the S1 C_{org} content is low, postdepositional oxidation of the original sapropel is insignificant, and no lower Mn zone exists. As a result, the zones of C_{org} enrichment and higher Ba/Al ratio coincide in this S1 [*Mercone et al.*, 2001]. Like the upper Mn zone in cores T87-29B (Figure 5) and BP15 (Figure 2) that were also retrieved from shallow water depths, the Mn zone (max. 3.3 wt % Mn) in core MD90-917 is within the S1 unit. Thus it is located in sediments laid down before the end of S1 times. However, this S1 unit is now located so deep in the sediments that the pore waters at this level must now be anoxic.

[37] X-ray diffraction of material from this Mn zone revealed a 2.94 Angstrom d-spacing peak characteristic for kutnahorite, an authigenic Mn-Ca carbonate mineral [*Mercone et al.*, 2001] (Figure 6). The diffusion of Mn^{2+} in carbonate oozes and marls in anoxic environment is often limited by the uptake of Mn^{2+} onto carbonate surfaces [*Boyle*, 1983; *Thomson et al.*, 1986; *Middelburg et al.*, 1987]. A rough estimate of the composition of the authigenic Mn-Ca carbonate in core MD90-917 was obtained by plotting the Ca and CO_3^{2-} contents against Mn content for samples from the Mn zone with Mn contents >0.5 wt %. The molar balance of additional Mn plus Ca versus additional CO_3^{2-} corresponds to $(Mn_{0.77}Ca_{0.23})CO_3$. This is similar to the Mn molar fraction of 0.7–0.8 found in the authigenic Mn-Ca carbonates that form episodically as laminations in the sediments of the Baltic Sea deeps. The critical requirement for the formation of these Baltic Sea Mn layers is the development of very high (>0.2 mmol kg^{-1}) pore water Mn^{2+} concentrations from MnO_x reduction in the presence of alkalinity [*Kulik et al.*, 2000; *Neumann et al.*, 2002]. The Mn zone in core MD90-917 shows that a conversion of MnO_x to kutnahorite also occurs in eastern Mediterranean sediments when MnO_x is reduced. Given the repetitive nature of sapropel formation, such an authigenic Mn-Ca carbonate zone can also be expected to have formed in the sedimentary record in association with older sapropels, although their long-term persistence is not assured [*Van Os et al.*, 1991, 1994; *De Lange et al.*, 1994; *Heiser et al.*, 2001].

[38] If adsorbed Mo is lost preferentially when MnO_x is reduced, as suggested by *Shimmield and Price* [1986], Mo would not be expected to incorporate into the kutnahorite. A clear Mo enrichment does coincide with the Mn enrichment, although the Mn/Mo mass ratio at and above this Mn zone averages $\sim$ 1700:1. This ratio is considerably larger than the Mn/Mo ratios observed in MnO_x in the cores discussed above where oxic conditions still exist (Figure 6). Loss of Mo from MnO_x on reduction therefore appears to have been extensive but not quantitative.

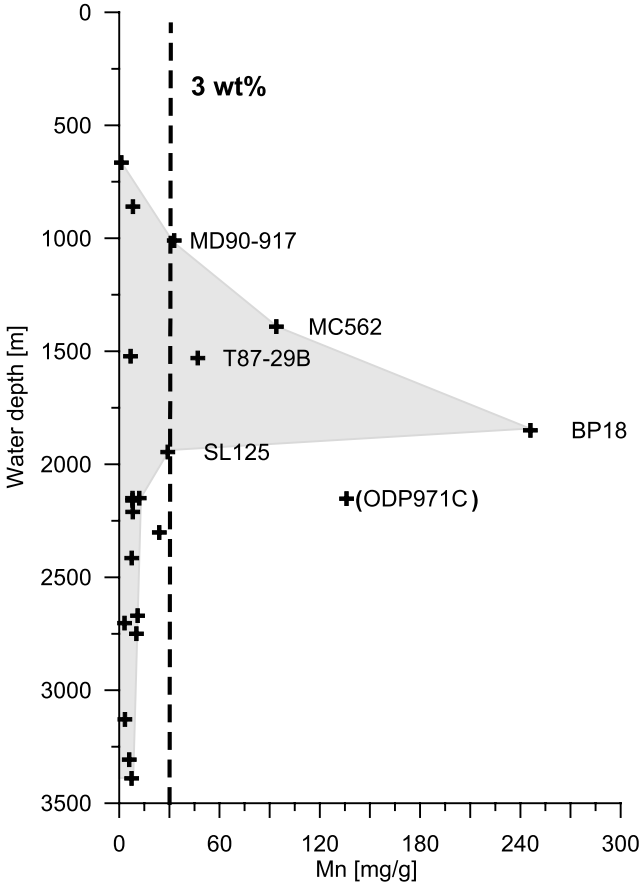

Figure 7. Maximum Mn content (mg g^{-1}) in the upper Mn zone of the cores studied versus water depth. Additional data from cores MC12 and 07S [*Thomson et al.*, 1995]; UM15, 26, and 35 [*Van Santvoort et al.*, 1996]; and LC21, BC12, LC25, and MDVAL90-9502 [*Mercone et al.*, 2000] are also shown. The dashed line is at 3 wt % Mn.

3.6. A Conceptual Model for Formation of the Upper Mn Layer Above Sapropel S1

[39] Some generalizations can be drawn from consideration of S1 sapropel units with an upper Mn zone with a maximum Mn content of >3 wt %:

[40] 1. Such large Mn concentrations are found at other eastern Mediterranean localities besides the crestal diapiric ridge (the Marker Bed area), e.g., on the Libyan slope, Medina Rise, and the Straits of Otranto (Figure 1).

[41] 2. Apart from core ODP971C (2152 m), all S1 units with unusually large upper peak Mn contents occur in sediments retrieved from water depths between 1100 and 2000 m (Figure 7). Not all cores from this water depth range exhibit a strongly Mn-enriched zone however, and Mn contents are highly variable in the two areas from which multiple cores are available, namely the Marker Bed area [*Cita et al.*, 1989; *De Capitani and Cita*, 1996; this work] and the Libyan slope (this work).

[42] 3. In the Libyan slope cores studied here, a benthic foraminiferal fauna is present throughout S1 in core MC562 from 1391 m [*Casford et al.*, 2003] but completely absent from the S1 unit of core BP18 from 1850 m. This indicates that bottom waters at the depth interval 1100–1800 m could not have been continuously anoxic during S1 formation.

[43] 4. The systematics of parallel Mo and Li enrichments with MnO_x are conspicuous in all cores containing the distinct upper Mn zone.

[44] It is commonly considered that solid-phase Mn enrichments in sediments result from the contact of oxic/anoxic interfaces in the water column with bottom topography [e.g., *Force and Cannon*, 1988; *Frakes and Bolton*, 1992; *Calvert and Pedersen*, 1996]. The accumulation of fine particulate MnO_x precipitated in the water column also results in variable localized Mn enrichments. Two independent lines of evidence suggest that it is likely that during S1 formation eastern Mediterranean surface sediments in deeper water had a lower redox potential than sediments in shallower water. *Murat and Got* [2000] found that the C_{org} of S1 units increased systematically between water depths of 500 and 4000 m and inferred that deeper sediments must have experienced lower mean bottom water O_2 levels than shallower sediments. *Casford et al.* [2003] noted that benthic foraminifera occur throughout S1 sapropel units in several cores retrieved from water depths <2000 m, and inferred that bottom waters must have been dysoxic or at least intermittently oxic.

[45] The combination of less intense or less frequent bottom water ventilation and higher preserved C_{org} contents in the deepest sediments during sapropel formation would be expected to lead to anoxia in the overlying bottom waters. Anoxia would consequently allow for the loss of considerable amounts of Mn^{2+} from the sediments to bottom waters and would promote sulfide formation. The presence of high O_2 values higher in the water column, either continuously or intermittently during S1 formation would be expected to precipitate this Mn^{2+} where and when oxic and anoxic waters met and mixed.

[46] In the present anoxic water column of the Black Sea, the highest dissolved Mn^{2+} contents occur in the few hundred meters below the redox interface that is located at ~200 m [e.g., *Lewis and Landing*, 1991]. This results from precipitation of MnO_x at the oxic/anoxic redox interface in the water column in response to mixing and diffusion, and from the continuous dissolution of precipitated MnO_x as it sinks back down into the deeper, anoxic sulfidic water column. *Kempe et al.* [1991] reported that a fine particle layer (FPL) with a large increase in dissolved Mn^{2+} below it follows the pycnocline in the Black Sea. This FPL also has higher concentrations of particulate manganese toward the shelf where MnO_x deposited in the sediment is exposed to reducing bottom waters. A similar process should be expected for the eastern Mediterranean during S1 times, but the geometry of the oxic/anoxic interface must have been quite different. Some level of ventilation to considerable depth is required to introduce O_2 at depth to react with deep anoxic waters containing Mn^{2+} and form MnO_x.

[47] Differences in oxygenation level with water depth during sapropel S1 formation thus readily provided a mechanism through which both a preferential loss of Mn^{2+} from the deepest sediments and a preferential deposition of MnO_x on higher topography in the basin might

have occurred. These differences in the mean oxygenation levels must have occurred throughout the time of S1 formation as indicated by the distribution of benthic foraminifera and the increasing C_{org} contents [*Casford et al.*, 2003; *Murat and Got*, 2000]. A single basin-wide ventilation event at the end of S1 times could not have caused the Mn distributions now observed in the sediments, nor produced the major upper Mn zone. However, the record of multiple hydrogenetically formed inputs of MnO_x to midwater depth (~1000–2000 m) sediments would not be preserved as spikes in Mn content in S1 sediments, because they would be dissolved by anoxic pore waters in the sapropel and concentrated into a single surficial diagenetic MnO_x layer. This process is exemplified by the upper narrow (~4 cm) strongly Mn-enriched zone in core ODP971C that sits at the top of the thick, largely redeposited S1 unit. This narrow upper Mn zone is consistent with the redistribution of Mn as MnO_x from within that unusually thick (redeposited) sapropel, which implies that bottom waters must have been oxic to some degree at the time of its formation late in S1 times.

[48] A one-dimensional, reactive transport model was used to evaluate our genetic model for the enrichment of Mn above S1 sediments in the eastern Mediterranean. First, S1 conditions were simulated by assuming that high dissolved Mn^{2+} and low dissolved O_2 concentrations (Table 3) existed at the sediment-water interface for a period of about 4100 years (Figure 8a). The results of this S1 model run were employed as the initial conditions for the post-S1 model runs. The first post-S1 model run tested if the upper high-Mn zone might have formed purely by diagenesis within the sediment. In order to simulate the shift from high Mn^{2+} concentrations during S1 to present-day conditions in the post-S1 model, an exponential function was used that "slowly" decreased the Mn flux at the lower boundary according to

$$\left[Mn^{2+}_{LB}\right](t) = \left([Mn_{S1}] - [Mn_{PD}]\right)\exp^{-0.0015t} + [Mn_{PD}], \tag{8}$$

where [Mn $_{S1}$] and [Mn $_{PD}$] is the concentration of Mn^{2+} during S1 (results of the S1 model run) and present-day, respectively.

[49] This model run simulates the possibility of MnO_x precipitation within the sediment at the transition from S1 to recent conditions, assuming fairly high dissolved Mn concentrations during S1 and a sudden shift to high oxygen and low Mn^{2+} levels at the sediment surface. The model results after 1000, 3000, and 5500 year simulations (Figures 8b–8d) show that pure sediment diagenesis could not have produced the high Mn values that have been found above the S1 horizon in sediments between 1000 and 2000 m water depth in the eastern Mediterranean.

[50] To simulate an exceptional situation similar to that favored in this paper, where the common interplay of increasing O_2 and decreasing Mn^{2+} in the bottom water is suppressed, a second post-S1 model run was adapted. This model run assumes a "slow" increase of O_2 accompanied by a slow decrease of Mn^{2+} over time at the sediment surface (thus in the bottom water; upper boundary conditions) by implementing the following exponential equations:

$$[O_{2UB}](t) = [O_{2\,S1}] + [O_2]\left(1 - \exp^{0.01t}\right) \tag{9}$$

and

$$\left[Mn^{2+}_{UB}\right](t) = \left[Mn^{2+}_{S1}\right] - 0.00005\exp^{-0.06t} + 0.00005, \tag{10}$$

where [$O_{2\ S1}$] and [O_2] are the corresponding concentration during S1 times (results of the S1 model run) and present-day at the sediment surface (Table 3). Since the recent eastern Mediterranean is a well-ventilated basin, the Mn^{2+} background concentration has been taken from the uppermost pore water sample (0.25 cm) of core BP18 at 0.00005 mmol dm^{-3}.

[51] This model run considers slowly decreasing Mn^{2+} concentrations as lower and upper boundary conditions as well as slowly increasing O_2 concentrations within the water column (upper boundary conditions) at the transition from S1 to recent time and consequently initiates enhanced MnO_x precipitation. The results after 1000, 3000, and 5500 year simulations produce an extreme MnO_x enrichment with the magnitude depending on the exponential factor in the exponential equations (Figures 8e–8g).

[52] Consequently, these model results confirm that the Mn in the upper zone is mainly diagenetic, even though it initially formed at intermediate water depth sites as a hydrogenetic precipitate. Indeed, the unusual strongly Mn-enriched upper zone occurs at and above the water depth (~2000 m), at which mud mounds are found in the eastern Mediterranean [*Robertson and Kopf*, 1998; *Kopf et al.*, 2000]. These mounds emit CH_4 and possibly Mn^{2+}, but a Mn^{2+} contribution from this source would be expected to oxidize to fine particulate MnO_x in the water column that would behave similarly to the hydrogenetic MnO_x just discussed [*Klinkhammer and Hudson*, 1986].

[53] A corollary of the mechanism envisaged is that sediments from the deepest parts of the basin are expected to have encountered the most marked sediment and bottom water anoxia and therefore to have lost the most Mn. All published profiles from cores at >2500 m water depth

Figure 8. Results of the reactive-transport model: (a) at the end of S1, (b–d) after 1, 3, and 5.5 kyr considering diagenetic processes within the sediment only, and (e–g) after 1, 3, and 5.5 kyr considering diagenetic processes within the sediment as well as slowly changing concentrations of O_2 and Mn^{2+} at the sediment-water interface. The shaded area indicates the residual S1 horizon. X axes (O_2, Mn^{2+}) apply for the upper and lower panel. The MnO_x concentrations in the upper and lower panel have separate x axes, except for the pair displaying the situation after 5.5 kyr; these show the measured values for MnO_x and Mn^{2+} (box core BP18) for comparison. Note that the MnO_x *x* axis of D/G contains a change of scale.

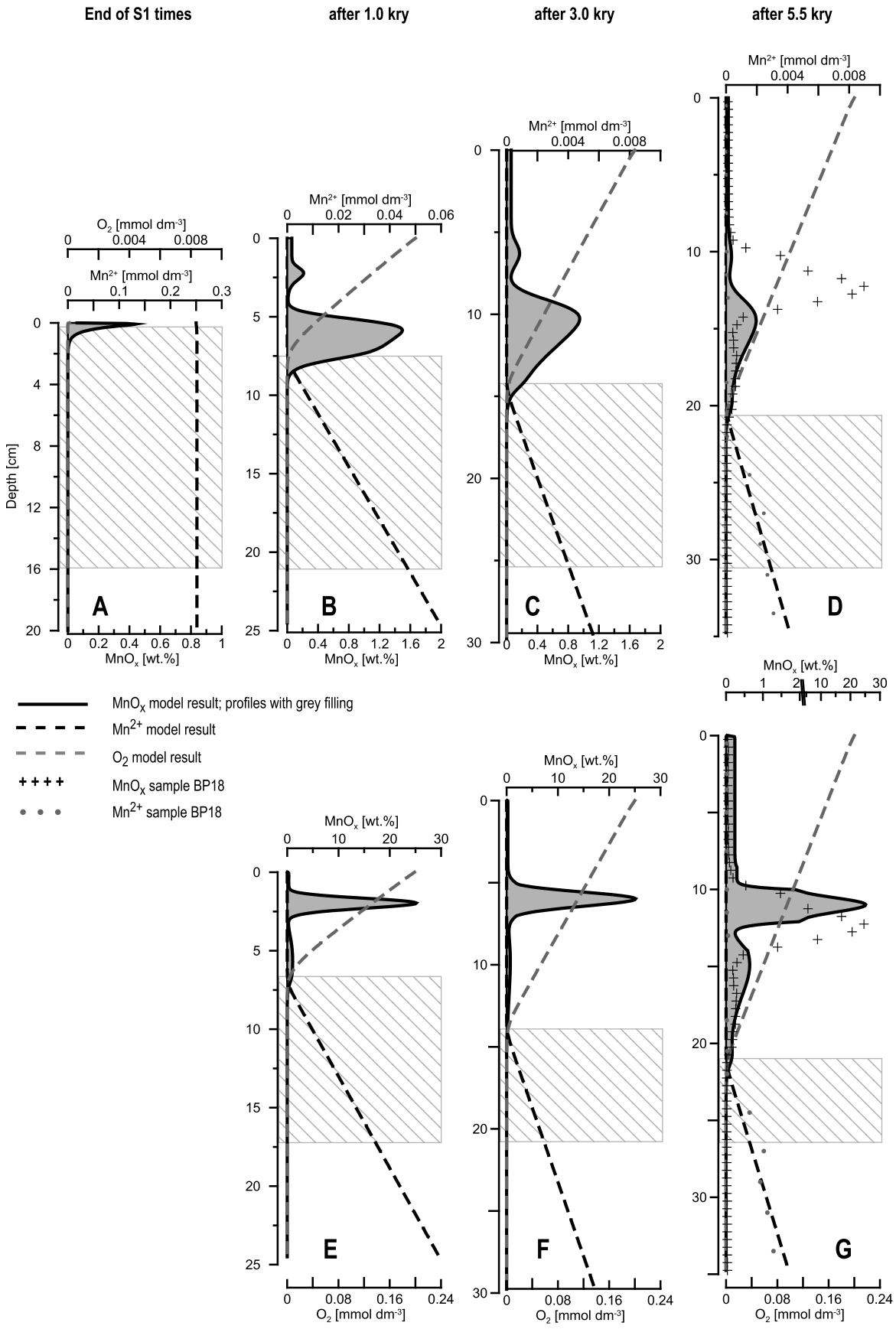
End of S1 times
after 1.0 kry
after 3.0 kry
after 5.5 kry
Depth [cm]
A
B
C
D
E
F
G
MnOx [wt.%]
Mn2+ [mmol dm-3]
O2 [mmol dm-3]
MnOx model result; profiles with grey filling
Mn2+ model result
O2 model result
MnOx sample BP18
Mn2+ sample BP18

Figure 8

exhibit upper Mn zone contents of <1 wt % (Figure 7), for example the deep-water core SL114 (Figure 2 and Table 1). On the other hand, higher mean O_2 concentrations in bottom waters at shallower water sites (cores BP15, T87-29B, MD90-917; Figure 2, 5, 6, and 7) can account for the occurrence of the upper Mn zone within, rather than overlying the S1 unit. Higher bottom water O_2 concentrations at these sites during sapropel formation would have resulted in deeper penetration of oxygen into the sediment. The available Mn in the sediments would then have been diagenetically enriched in this deeper oxic layer, within the sapropel, rather than at the very top of the sapropel.

4. Conclusions

[54] A set of cores with large (>3 wt %) Mn contents in the uppermost of two Mn-enriched horizons that are usually observed above sapropel S1 have been examined in the light of other S1 studies. Although mostly equivalent in time to the smaller upper Mn zone, the magnitude of the large Mn zone appears variable within particular areas. The wide variation in Mn content does not appear to be reflected in other geochemical parameters apart from elements associated with the MnO_x. Our preferred scenario involves a diagenetic release of Mn^{2+} from the deepest water (>2000 m) sediments into anoxic bottom waters, a reprecipitation of this Mn^{2+} as particulate MnO_x where it encounters O_2 higher in the water column, and a removal of the particulate MnO_x onto higher topography underlying oxic waters. The precipitation step occurs when anoxic and oxic waters meet at intermediate water depths (1000–2000 m). This mechanism is consistent with higher mean O_2 levels at intermediate depths than at the deepest depths in the basin, which is also indicated by micropaleontological and C_{org} evidence. This situation must also have occurred regularly during sapropel formation rather than in a single event at the end of the S1 period, because benthic foraminifera and lower C_{org} contents are found throughout S1 units formed at shallower water depths. The combination of pore water anoxia in sapropel surface sediments and some level of oxygen in the overlying bottom water would maintain the excess Mn introduced by this hydrogenetic mechanism as a large diagenetic zone in sediments at midwater depth (~1000–2000 m). Model results indicate that this extreme Mn enrichment can form only by slowly decreasing Mn^{2+} and slowly increasing O_2 supplies at the sediment surface. This emphasizes MnO_x formation within the water column or at the sediment/water boundary. Molybdenum and lithium are incorporated into this diagenetic MnO_x at Mn:Mo and Mn:Li ratios that vary near 600:1 and 750:1, and with a $\delta^{98/95}Mo_{MOMO}$ ratio of ~−2.5 ‰. These ratios and isotopic composition support our preferred scenario.

[55] **Acknowledgments.** We are grateful to Sebastian Meier (Natural History Museum, London), Simon Troelstra (Free University, Amsterdam), Martine Paterne (LSCE, Gif-sur-Yvette), and Eelco Rohling (SOC) for the provision of samples (cores MC562, T87-29B, MD90-917, and ODP971C, respectively). Two anonymous reviewers are thanked for their valuable comments. Robin Keir is gratefully acknowledged for constructive comments and thorough editing of the text. Caroline Slomp is thanked for discussions on SAP project data. We thank Darryl Green, Thomas Appel, Helen de Waard, Eric van Vilsteren, and Rinske Knoop for their contribution to laboratory analysis and the crew and the shipboard parties of the cruises named in Table 1 for their contribution to sample collection. Thomas Nägler (University Bern) and Christoph Vogt (University of Bremen) are acknowledged for the molybdenum isotope and XRD measurements, respectively. This work was partly funded by EU-MAST-III project MAS3-CT97-0137, Sapropels and Paleoproductivity (SAP); NWO project Sapropel-related Paleoceanographic Studies in Sediments of the eastern Mediterranean (SAPS). This is NSG contribution 2006 0987).

References

Balzer, W. (1982), On the distribution of iron and manganese at the sediment water interface: Thermodynamic versus kinetic control, *Geochim. Cosmochim. Acta*, *46*, 1153–1162.

Bertine, K. K., and K. K. Turekian (1973), Molybdenum in marine deposits, *Geochim. Cosmochim. Acta*, *37*, 1415–1434.

Béthoux, J. P. (1993), Mediterranean sapropel formation, dynamic and climatic viewpoints, *Oceanol. Acta*, *16*, 127–133.

Boudreau, B. (1996), A method-of-lines code for carbon and nutrient diagenesis in aquatic sediments, *Comput. Geosci.*, *22*, 479–496.

Boyle, E. A. (1983), Manganese carbonate overgrowths on foraminifera tests, *Geochim. Cosmochim. Acta*, *47*, 1815–1819.

Calvert, S. E., and T. F. Pedersen (1993), Geochemistry of Recent oxic and anoxic marine sediments: Implications for the geological record, *Mar. Geol.*, *113*, 67–88.

Calvert, S. E., and T. F. Pedersen (1996), Sedimentary geochemistry of manganese: Implications for the environment of formation of manganiferous black shales, *Econ. Geol. Bull. Soc.*, *91*, 36–47.

Camerlenghi, A., M. B. Cita, W. Hieke, and T. Ricchiuto (1992), Geological evidence for mud diapirism on the Mediterranean Ridge accretionary complex, *Earth Planet Sci. Lett.*, *109*, 493–504.

Casford, J. S. L., E. J. Rohling, R. H. Abu-Zied, C. Fontanier, F. J. Jorissen, M. J. Leng, G. Schmiedl, and J. Thomson (2003), A dynamic concept for eastern Mediterranean circulation and oxygenation during sapropel formation, *Palaeogeogr. Palaeoclimatol. Palaeoecol.*, *190*, 103–119.

Cita, M. B., F. Aghib, S. Arosio, S. Folco, L. Sarto, E. Erba, and A. Rizzi (1989), Bacterial colonies and manganese micronodules related to fluid escape on the crest of the Mediterranean Ridge, *Riv. Ital. Paleontol. Stratigr.*, *95*, 315–336.

Crusius, J., S. Calvert, T. Pedersen, and D. Sage (1996), Rhenium and molybdenum enrichments in sediments as an indicator of oxic, suboxic and sulfidic conditions of deposition, *Earth Planet. Sci. Lett.*, *145*, 65–78.

De Capitani, L., and M. B. Cita (1996), The "marker bed" of the Mediterranean Ridge diapiric belt: Geochemical characteristics, *Mar. Geol.*, *132*, 215–225.

Dekov, V. M., V. Marchig, I. Rajta, and I. Uzonyi (2003), Fe-Mn micronodules born in the metalliferous sediments of two spreading centres: The East Pacific Rise and Mid-Atlantic Ridge, *Mar. Geol.*, *199*, 101–121.

De Lange, G. J. (1992), Distribution of various extracted phosphorus compounds in the interbedded turbiditic/pelagic sediments of the Madeira Abyssal Plain, eastern North Atlantic, *Mar. Geol.*, *109*, 115–139.

De Lange, G. J., J. J. Middelburg, and P. A. Pruysers (1989), Discussion: Middle and Late Quarternary depositional sequences and cycles in the eastern Mediterranean, *Sedimentology*, *36*, 151–158.

De Lange, G. J., G. Catalano, G. P. Klinkhammer, and G. W. Luther III (1990), The interface between oxic seawater and the anoxic Bannock brine; its sharpness and the consequences for the redox-related cycling of Mn and Ba, *Mar. Chem.*, *31*, 205–217.

De Lange, G. J., B. van Os, P. A. Pruysers, J. J. Middelburg, D. Castradori, P. van Santvoort, P. J. Müller, H. Eggenkamp, and F. G. Prahl (1994), Possible early diagenetic alteration of palaeo proxies, in *Carbon Cycling in the Glacial Ocean: Constraints on the Ocean's Role in Global Change*, *NATO ASI Ser., Ser. I*, vol. 17, edited by R. Zahn et al., pp. 225–258, Springer, New York.

De Lange, G. J., P. J. M. van Santvoort, C. Langereis, J. Thomson, C. Corselli,

A. Michard, M. Rossignol-Strick, M. Paterne, and G. Anastasakis (1999), Palaeo-environmental variations in eastern Mediterranean sediments: A multidisciplinary approach in a prehistoric setting, *Prog. Oceanogr.*, *44*, 369–386.

Force, E. R., and W. F. Cannon (1988), Depositional model for shallow-marine manganese deposits around black shale deposits, *Econ. Geol. Bull. Soc.*, *83*, 93–117.

Frakes, L., and B. Bolton (1992), Effects of ocean chemistry, sea-level and climate on the formation of primary sedimentary manganese ore deposits, *Econ. Geol. Bull. Soc.*, *87*, 1207–1217.

Gieskes, J. M. (1983), The chemistry of interstitial waters of deep sea sediments: Interpretation of deep sea drilling data, in *Chemical Oceanography*, vol. 8, edited by J. P. Riley and R. Chester, pp. 221–269, Elsevier, New York.

Glasby, G. P., D. Stüben, G. Jeschke, P. Stoffers, and C.-D. Garbe-Schönberg (1997), A model for the formation of hydrothermal manganese crusts from the Pitcairn Island hotspot, *Geochim. Cosmochim. Acta*, *61*, 4583–4597.

Heiser, U., T. Neumann, J. Scholten, and D. Stüben (2001), Recycling of manganese from anoxic sediments in stagnant basins by seawater inflow: A study of surface sediments from the Gotland Basin, *Baltic Sea, Mar. Geol.*, *177*, 151–166.

Helz, G. R., C. V. Miller, J. M. Charnock, J. F. M. Mosselmans, R. A. D. Pattrick, C. D. Gardner, and D. J. Vaughan (1996), Mechanism of molybdenum removal from the sea and its concentration in black shales: EXAFS evidence, *Geochim. Cosmochim. Acta*, *60*, 3631–3642.

Hem, J. D. (1972), Chemical factors that influence the availability of iron and manganese in aqueous systems, *Geol. Soc. Am. Bull.*, *83*, 443–450.

Hensen, C., and K. Wallmann (2005), Methane formation at Costa Rica continental margin: Constraints for gas hydrate inventories and cross-décollement fluid flow, *Earth Planet. Sci. Lett.*, *236*, 41–60.

Hieke, W., M. B. Cita, G. L. Mirabile, A. Negri, and F. Werner (1996), The summit area (Antaeus/Pan di Zucchero) of the Mediterranean Ridge: A mud diaper field?, *Mar. Geol.*, *132*, 113–129.

Higgs, N. C., J. Thomson, T. R. S. Wilson, and I. W. Croudace (1994), Modification and complete removal of eastern Mediterranean sapropel by postdepositional oxidation, *Geology*, *22*, 423–426.

Hilgen, F. J. (1991), Astronomical calibration of Gauss to Matuyama sapropels in the Mediterranean and implication for the Geomagnetic Polarity Time Scale, *Earth Planet. Sci. Lett.*, *104*, 226–244.

Hodkinson, R. A., P. Stoffers, J. Scholten, D. S. Cronan, G. Jeschke, and T. D. S. Rogers (1994), Geochemistry of hydrothermal manganese deposits from the Pitcairn Island hotspot, southeastern Pacific, *Geochim. Cosmochim. Acta*, *58*, 5011–5029.

Huckriede, H., and D. Meischner (1996), Origin and environment of manganese-rich sediments within black-shale basins, *Geochim. Cosmochim Acta*, *60*, 1399–1413.

Huerta-Diaz, M. A., and J. W. Morse (1992), Pyritization of trace metals in anoxic marine sediments, *Geochim. Cosmochim. Acta*, *56*, 2681–2702.

James, R. H., and M. R. Palmer (2000), Marine geochemical cycles of the alkali elements and boron: The role of sediments, *Geochim. Cosmochim. Acta*, *64*, 3111–3122.

Kadko, D., J. K. Cochran, and M. Lyle (1987), The effect of bioturbation and adsorption gradients on solid and dissolved radium profiles in sediments from the eastern equatorial Pacific, *Geochim. Cosmochim. Acta*, *51*, 1613–1623.

Kempe, S., A.-R. Diercks, G. Liebezeit, and A. Prange (1991), Geochemical and structural aspects of the pycnocline in the Black Sea (R/V *Knorr* 134-8 Leg 1, 1988), in *Black Sea Oceanography*, edited by E. Izdar and J. W. Murray, pp. 89–110, Springer, New York.

Klinkhammer, G., and A. Hudson (1986), Dispersal patterns for hydrothermal plumes in the south-Pacific using manganese as a tracer, *Earth Planet. Sci. Lett.*, *79*, 241–249.

Kopf, A., A. H. F. Robertson, and N. Volkmann (2000), Origin of mud breccia from the Mediterranean Ridge accretionary complex based on evidence of the maturity of organic matter and related petrographic and regional tectonic evidence, *Mar. Geol.*, *166*, 65–82.

Koschinsky, A., and P. Halbach (1995), Sequential leaching of marine ferromanganese precipitates: Genetic implications, *Geochim. Cosmochim. Acta*, *59*, 5113–5132.

Koschinsky, A., and J. R. Hein (2003), Uptake of elements from seawater by ferromanganese crusts: Solid-phase associations and seawater speciation, *Mar. Geol.*, *198*, 331–351.

Kostka, J. E., and G. W. Luther III (1994), Partitioning and speciation of solid phase iron in saltmarsh sediments, *Geochim. Cosmochim. Acta*, *58*, 1701–1710.

Kristensen, E., K. D. Kristiansen, and M. H. Jensen (2003), Temporal behavior of manganese and iron in a sandy coastal sediment exposed to water column anoxia, *Estuaries*, *26*(3), 690–699.

Kulik, D. A., M. Kersten, U. Heiser, and T. Neumann (2000), Application of Gibbs energy minimization to model early-diagenetic solid-solution aqueous-solution equilibria involving authigenic rhodochrosites in anoxic Baltic Sea sediments, *Aquat. Geochem.*, *6*, 147–199.

Lewis, B. L., and W. M. Landing (1991), The biogeochemistry of manganese and iron in the Black-Sea, *Deep Sea Res., Part A*, *38*, 773–803.

Lord, C. J. III (1982), A selective and precise method for pyrite determination in sedimentary materials, *J. Sediment. Petrol.*, *52*, 664–666.

Lourens, L. J., A. Antonarakou, F. J. Hilgen, and A. A. M. van Hoof (1996), Evaluation of the Plio-Pleistocene astronomical timescale, *Paleoceanography*, *11*, 391–413.

Lynn, D. C., and E. Bonatti (1965), Mobility of manganese in diagenesis of deep-sea sediments, *Mar. Geol.*, *3*, 457–474.

Mercone, D., J. Thomson, I. W. Croudace, G. Siani, M. Paterne, and S. Troelstra (2000), Duration of S1, the most recent sapropel in the eastern Mediterranean Sea, as indicated by AMS radiocarbon and geochemical evidence, *Paleoceanography*, *15*, 336–347.

Mercone, D., J. Thomson, R. H. Abu-Zied, I. W. Croudace, and E. J. Rohling (2001), High-resolution geochemical and micropalaeontological profiling of the most recent eastern Mediterranean sapropel, *Mar. Geol.*, *177*, 25–44.

Middelburg, J. J., G. J. de Lange, and C. H. van der Weijden (1987), Manganese solubility control in marine pore waters, *Geochim. Cosmochim. Acta*, *51*, 759–763.

Mills, R. A., and H. Elderfield (1995), Hydrothermal activity and the geochemistry of metalliferous sediment, in *Seafloor Hydrothermal Systems: Physical, Chemical, Biological and Geological Interactions*, *Geophys. Monogr. Ser.*, vol. 91, edited by S. Humphris et al., pp. 392–407, AGU, Washington, D. C.

Morford, J. J., and S. R. Emerson (1999), The geochemistry of redox sensitive trace metals in sediments, *Geochim. Cosmochim. Acta*, *63*, 1735–1750.

Murat, A., and H. Got (2000), Organic carbon variations of the eastern Mediterranean Holocene sapropel: A key for understanding formation processes, *Palaeogeogr. Palaeoclimatol. Palaeoecol.*, *158*, 241–257.

Neumann, T., U. Heiser, M. A. Leosson, and M. Kersten (2002), Early diagenetic processes during Mn-carbonate formation: Evidence from the isotopic composition of authigenic Ca-rhodochrosite of the Baltic Sea, *Geochim. Cosmochim. Acta*, *66*, 867–879.

Passier, H. F., J. J. Middelburg, B. J. H. van Os, and G. J. de Lange (1996), Diagenetic pyritisation under eastern Mediterranean sapropels caused by downward sulfide diffusion, *Geochim. Cosmochim. Acta*, *60*, 751–763.

Passier, H. F., G. J. de Lange, and M. J. Dekkers (2001), Magnetic properties and geochemistry of the active oxidation front and the youngest sapropel in the eastern Mediterranean Sea, *Geophys. J. Int.*, *145*, 604–614.

Pruysers, P. A., G. J. de Lange, J. J. Middelburg, and D. J. Hydes (1993), The diagenetic formation of metal-rich layers in sapropel-containing sediments in the eastern Mediterranean, *Geochim. Cosmochim. Acta*, *37*, 527–536.

Rasmussen, T. L. (1991), Benthonic and planktonic foraminifera in relation to the early Holocene stagnation in the Ionian Basin, central Mediterranean, *Boreas*, *20*, 357–376.

Reitz, A., C. Hensen, S. Kasten, J. A. Funk, and G. J. de Lange (2004a), A combined geochemical and rock-magnetic investigation of a redox horizon at the last glacial/interglacial transition, *Phys. Chem. Earth*, *29*, 921–931.

Reitz, A., K. Pfeifer, G. J. de Lange, and J. Klump (2004b), Biogenic barium and the detrital Ba/Al ratio: A comparison of their direct and indirect determination, *Mar. Geol.*, *204*, 289–300.

Reitz, A., J. Thomson, G. J. de Lange, D. R. H. Green, C. P. Slomp, and A. C. Gebhardt (2006), Effects of the Santorini (Thera) eruption on manganese behavior in Holocene sediments of the eastern Mediterranean, *Earth Planet. Sci. Lett.*, *241*, 188–201.

Robertson, A. H. F., and A. Kopf (1998), Tectonic setting and processes of mud volcanism on the Mediterranean Ridge accretionary complex: Evidence from Leg 160, in *Proc. Ocean Drill. Program Sci. Results*, *160*, 665–680.

Roether, W., and R. Well (2001), Oxygen consumption in the eastern Mediterranean, *Deep Sea Res., Part I*, *48*, 1535–1551.

Rohling, E. J. (1994), Review and new aspects concerning the formation of eastern Mediterranean sapropels, *Mar. Geol.*, *122*, 1–28.

Rossignol-Strick, M. (1985), Mediterranean Quarternary sapropels: An immediate response to orbital insolation, *Nature*, *304*, 46–49.

Roy, S. (1992), Environments and processes of manganese deposition, *Econ. Geol. Bull. Soc.*, *87*, 1218–1236.

Rutten, A., and G. J. de Lange (2002), A novel selective extraction of barite, and its applica-

tion to eastern Mediterranean sediments, *Earth Planet. Sci. Lett.*, *198*, 11–24.

Rutten, A., and G. J. de Lange (2003), Sequential extraction of iron, manganese and related elements in S1 sapropel sediments, eastern Mediterranean, *Palaeogeogr. Palaeoclimatol. Palaeoecol.*, *190*, 79–101.

Rutten, A., G. J. de Lange, A. Hayes, E. J. Rohling, A. F. M. de Jong, and K. van der Borg (1999), Deposition of sapropel S1 sediments in oxic pelagic and anoxic brine environments in the eastern Mediterranean: Differences in diagenesis and preservation, *Mar. Geol.*, *153*, 319–335.

Ruttenberg, K. C. (1992), Development of a sequential extraction method of different forms of phosphorus in marine sediments, *Limnol. Oceanogr.*, *37*, 1460–1482.

Sato, Y., S. Okabe, and N. Takematsu (1989), Major elements in manganese and iron oxides precipitated from seawater, *Geochim. Cosmochim. Acta*, *53*, 1883–1887.

Shimmield, G. B., and N. B. Price (1986), The behaviour of molybdenum and manganese during early sediment diagenesis: Offshore Baja California, Mexico, *Mar. Chem.*, *19*, 261–280.

Siebert, C., T. F. Nägler, and J. D. Kramers (2001), Determination of molybdenum isotope fractionation by double-spike multicollector inductively coupled plasma mass spectrometry, *Geochem. Geophys. Geosyst.*, *2*(7), doi:10.1029/2000GC000124.

Siebert, C., T. F. Nägler, F. von Blanckenburg, and J. D. Kramers (2003), Molybdenum isotope record as a potential new proxy for paleoceanography, *Earth Planet. Sci. Lett.*, *211*, 159–171.

Sternbeck, J., and G. Sohlenius (1997), Authigenic sulfide and carbonate mineral formation in Holocene sediments of the Baltic Sea, *Chem. Geol.*, *135*, 55–73.

Sundby, B., P. Martinez, and C. Gobeil (2004), Comparative geochemistry of cadmium, rhenium, uranium, and molybdenum in continental margin sediments, *Geochim. Cosmochim. Acta*, *68*, 2485–2493.

Takematsu, N., Y. Sato, S. Okabe, and E. Nakayama (1985), The partition of vanadium and molybdenum between manganese oxides and sea water, *Geochim. Cosmochim. Acta*, *49*, 2395–2399.

Thomson, J., N. C. Higgs, I. Jarvis, D. J. Hydes, S. Colley, and T. R. S. Wilson (1986), The behaviour of manganese in Atlantic carbonate sediments, *Geochim. Cosmochim. Acta*, *50*, 1807–1818.

Thomson, J., N. C. Higgs, R. R. S. Wilson, I. W. Croudace, G. J. de Lange, and P. J. M. van Santvoort (1995), Redistribution and geochemical behaviour of redox-sensitive elements around S1, the most recent eastern Mediterranean sapropel, *Geochim. Cosmochim. Acta*, *59*, 3487–3501.

Thomson, J., D. Mercone, G. J. de Lange, and P. J. M. van Santvoort (1999), Review of recent advances in the interpretation of Eastern Mediterranean sapropel S1 from geochemical evidence, *Mar. Geol.*, *153*, 77–89.

Totland, M., I. Jarvis, and K. E. Jarvis (1992), An assessment of dissolution techniques for the analysis of geological samples by plasma spectroscopy, *Chem. Geol.*, *95*, 35–62.

Troelstra, S. R., G. M. Ganssen, K. van der Borg, and A. F. M. de Jong (1991), A late Quaternary stratigraphic framework for eastern Mediterranean sapropel S1 based on AMS ^{14}C dates and stable oxygen isotopes, *Radiocarbon*, *33*(1), 15–21.

Tuenter, E., S. L. Weber, F. J. Hilgen, and L. J. Lourens (2003), The response of the African summer monsoon to remote and local forcing due to precession and obliquity, *Glob. Planet. Change*, *36*, 219–235.

Van der Weijden, C. H. (2002), Pitfalls of normalization of marine geochemical data using a common divisor, *Mar. Geol.*, *184*, 167–187.

Van Os, B. J. H., J. J. Middelburg, and G. J. de Lange (1991), Possible diagenetic mobilization of barium in sapropelic sediments from the eastern Mediterranean, *Mar. Geol.*, *100*, 125–136.

Van Os, B. J. H., L. Lourens, F. J. Hilgen, and G. J. de Lange (1994), The formation of Pliocene sapropels and carbonate cycles: Dilution, diagenesis and productivity, *Paleoceanography*, *9*, 601–617.

Van Santvoort, P. J. M., G. J. de Lange, J. Thomson, H. Cussen, T. R. S. Wilson, M. D. Krom, and K. Ströhle (1996), Active post-depositional oxidation of the most recent sapropel (S1) in sediments of the eastern Mediterranean Sea, *Geochim. Cosmochim. Acta*, *60*, 4007–4027.

Van Santvoort, P. J. M., G. J. de Lange, J. Thomson, S. Colley, F. J. R. Meysman, and C. P. Slomp (2002), Oxidation and origin of organic matter in surficial eastern Mediterranean hemipelagic sediments, *Aquat. Geochem.*, *8*, 153–175.

Vorlicek, T. P., and G. R. Helz (2002), Catalysis by mineral surfaces: Implications for Mo geochemistry in anoxic environments, *Geochim. Cosmochim. Acta*, *66*, 3679–3692.

Zhang, L., L.-H. Chan, and J. M. Gieskes (1998), Lithium isotope geochemistry of pore waters from Ocean Drilling Program sites 918 and 919, Irminger Basin, *Geochim. Cosmochim. Acta*, *62*, 2437–2450.

G. J. de Lange, Department of Earth Sciences-Geochemistry, Faculty of Geosciences, Utrecht University, P.O. Box 80021, NL-3508 TA Utrecht, Netherlands.

C. Hensen, SFB574, Christian-Albrecht University Kiel, Wischhofstr. 1-3, D-24148 Kiel, Germany.

A. Reitz, IFM-GEOMAR, Wischhofstr. 1-3, D-24148 Kiel, Germany. (areitz@ifm-geomar.de)

J. Thomson, Southampton Oceanography Centre, Empress Dock, Southampton SO14 3ZH, UK.